ACS APPLIED MATERIALS & INTERFACES

Research Article

www.acsami.org

Barbituric Acid-Based Magnetic *N*-Halamine Nanoparticles as Recyclable Antibacterial Agents

Alideertu Dong,*[,†] Yue Sun,[†] Shi Lan,[‡] Qin Wang,[†] Qian Cai,[†] Xiuzhen Qi,[†] Yanling Zhang,[†] Ge Gao,[‡] Fengqi Liu,[‡] and Chokto Harnoode*[,†]

[†]College of Chemistry and Chemical Engineering, Inner Mongolia University, Hohhot 010021, People's Republic of China

[‡]College of Chemistry, Jilin University, Changchun 130021, People's Republic of China

Supporting Information

ABSTRACT: Novel recyclable bactericidal materials, barbituric acid-based magnetic *N*-halamine nanoparticles (BAMNH NPs), were fabricated by coating of magnetic silica nanoparticles (MS NPs) with barbituric acid-based *N*-halamine by the aid of the radical polymerization. The sterilizing effect on the bacterial strain is investigated by incubating Gram-negative bacteria (*Escherichia coli* and *Pseudomonas aeruginosa*) and Gram-positive bacteria (*Staphylococcus aureus* and *Bacillus subtilis*). The as-prepared BAMNH NPs exhibit higher biocidal activity than the bulk powder barbituric acid-based *N*-halamine due to the high activated surface area. The structural effect of *N*-halamine on antimicrobial performance was fully clarified through the comparison between BAMNH NPs and hydantoin-based magnetic *N*-halamine nanoparticles (HMNH NPs). BAMNH NPs exhibited promising stability toward repeated washing and long-term storage. BAMNH NPs with different chlorine content were comparatively chosen to investigate the influence of chlorine content on the antimicrobial activity. An antibacterial recycle experiment revealed that no significant change occurred in the structure and antibacterial efficiency of BAMNH NPs after five recycle experiments. The combination of barbituric acid-based *N*-halamine with magnetic component results in an obvious synergistic effect and facilitates the repeated antibacterial applications, providing potential and ideal candidates for sterilization or even for the control of disease.

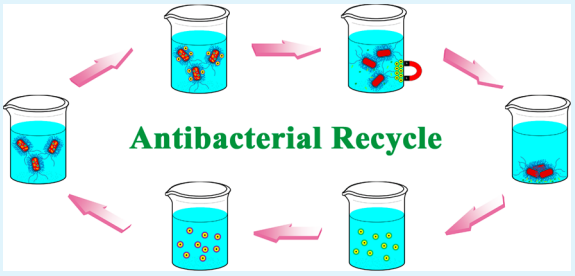

KEYWORDS: *barbituric acid, N-halamine, antibacterial, magnetic, recyclable*

INTRODUCTION

The microorganisms in environment are closely related to human health. It is thus indispensable to perform research into aspects of sterilization, prevention, disinfection, etc., to control disease.[1,2] Recently, sterilization is generally based on chemical antibacterial agents.[3] *N*-Halamine antibacterial materials are attracting continuous interest because of their peculiar properties, including powerful antibacterial activity, high durability, long-term stability, and regenerability.[4−6] The application of *N*-halamine antibacterial materials refers to the field of water purification systems, food storage and packaging, medical devices, hospital, hygienic products, dental office equipment, household sanitation, etc. As a contact biocide, the antibacterial efficiency of *N*-halamine antibacterial materials is closely related to their activated contact area with the bacteria. Obviously, the antibacterial efficiency proportionally increases with the activated contact area increase. Compared with traditional materials, nanometer-sized materials have their natural characteristics because they possess smaller size and larger surface area.[7] Therefore, the antibacterial activity of *N*-halamine can be improved efficiently by decreasing materials' size even into nanometer size.

N-Halamines with a nitrogen−halogen covalent bond in structure are always prepared by halogenating their corresponding precursor amide/imide/amino containing compounds.[8] It is well known that barbituric acid derivatives famous for the pharmaceutical and biological effect are promising heterocyclic compounds with two imide functional groups in the structure, which can work as the *N*-halamine precursor.[9] By halogenating the imide group, the as-synthesized barbituric acid-based *N*-halamines can be a potential candidate with excellent antibacterial properties. Nevertheless, reports of *N*-halamine antibacterial agents based on barbituric acid derivatives are quite rare.[10−12]

N-Halamines unlike other antibacterial materials have a unique feature of regenerability.[13] *N*-Halamines convert to amide, imide, or amino containing precusor as they contact with the microorganism, and they can return back to *N*-halamine structures after another chlorination treatment. Unfortunately, the repeated application of *N*-halamine materials is always hindered by their recovery problem. Antibacterial behavior of *N*-halamine materials utilized with the dispersed form is always performed in an aqueous suspension, which requires an extra procedure and further expense to recover

Received: June 6, 2013
Accepted: August 5, 2013
Published: August 5, 2013

   dx.doi.org/10.1021/am402191j | ACS Appl. Mater. Interfaces 2013, 5, 8125−8133

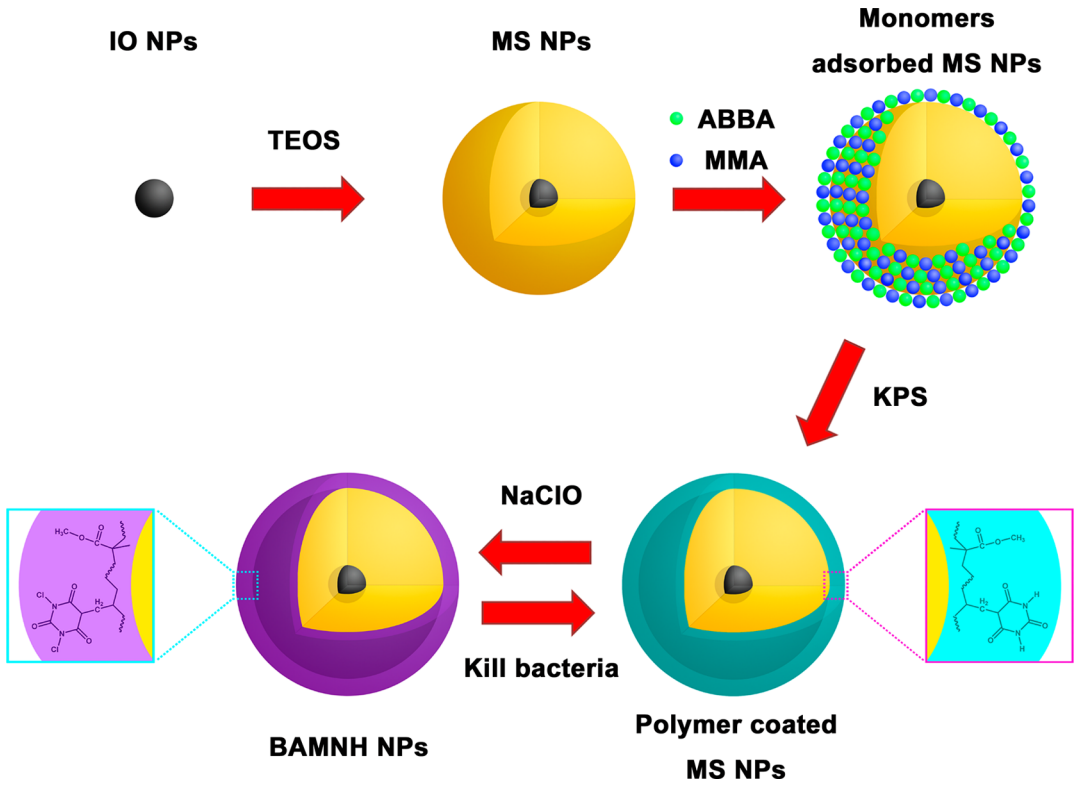

Figure 1. Schematic depiction of the synthetic procedure of BAMNH NPs.

them from suspension. To solve this problem, designative preparation of *N*-halamine materials with easy harvesting property is highly desirable for recyclable antibacterial applications.

Recently, researchers paid much more attention to magnetic nanoparticles owing to their unique characteristics, such as easy handling, good biocompatibility, low cytotoxicity, low cost, and eco-friendly performance.[14] In particular, the recyclable and localizing properties of magnetic nanoparticles by applied external magnetic field can facilitate the target recovery.[15,16] However, the utilization of magnetic nanoparticles is seriously limited because of the magnetically induced aggregation, surface oxidation, and deficiency of functional groups.[17,18] Therefore, magnetic nanoparticles were always encapsulated with silica by using various synthetic methods, protecting them from aggregation and surface oxidation to increase their stability.[19−21] In particular, magnetic silica nanoparticles (MS NPs) have revealed immense potential applications such as bioseparation, biosensor, field-induced assembly, enzyme immobilization, and catalysis due to their good stability, magnetic responsivity, low cytotoxicity, chemically modifiable surface, and ease of preparation.[22,23]

In this paper, we present the facile synthesis of novel magnetic *N*-halamine nanoparticles as promising antibacterial agents through the functionalization of magnetic silica nanoparticles with barbituric acid-based *N*-halamine. We chose barbituric acid-originated *N*-halamine as the polymer shell for antibacterial properties and a silica component as a stabilizer for nonaggregated magnetic nanoparticles. Introduction of the magnetic component into antibacterial materials can make the product reusable. Therefore, it is expected that the barbituric acid-based magnetic *N*-halamine nanoparticles have outstanding biocidal activity with easily recyclable magnetic behavior.

EXPERIMENTAL SECTION

Materials. Potassium persulfate (KPS) and methyl methacrylate were purchased from Shanghai Chemical Reagent Plant and Tianjin Chemical Reagent Plant, respectively. Sodium and urea were provided from Nanjing Chemical Reagent Co., Ltd. Hydrochloric acid, anhydrous methanol, tetrahydrofuran, hexane, diethyl ether, and acetone were obtained from Beijing Chemical Company. Sodium hydride (55% in oil) was purchased from Beijing Hengye Zhongyuan Chemical Co., Ltd. Diethyl malonate, allyl bromide, magnesium sulfate, sodium chloride, and sodium hypochlorite were available from Sinopharm Chemical Reagent Co., Ltd.

Preparation of 5-Allylbarbituric Acid. About 3.2 g of diethyl malonate was added dropwise into a 50 mL suspension of NaH (0.92 g) in THF at 0 °C, and the mixture was vigorously stirred at 25 °C for 1 h. After that, 2.90 g of allyl bromide was added into the above-mentioned mixture and stirred ceaselessly for 12 h. The resultant product was extracted with diethyl ether after adding 100 mL of water, and the organic layer was separated and collected after the washing with aqueous sodium chloride solution. The as-prepared crude product was purified with hexane/diethyl ether (10:1) mixed solvent by the column chromatography method.[24] A mixture containing dry sodium methoxide [prepared from sodium (0.2875 g) and methanol (7.5 mL)], 0.75 g of urea, 2.5 g of diethyl allylamlonate, and 2.5 mL of acetone was refluxed under the condition of vigorous stirring for 7 h. The product was treated successively through filtration, acetone washing, water suspending, and acidification with concentrated aqueous hydrochloric acid to pH 1−2. The filtered product was recrystallized by using ethanol to obtain 5-allylbarbituric acid as colorless needles.[25]

Preparation of Iron Oxide Nanoparticles. An improved chemical coprecipitation method was utilized to synthesize iron oxide nanoparticles (IO NPs).[26] Typically, a mixture of 1.817 g of $FeCl_3$ and 1.113 g of $FeCl_2{\cdot}4H_2O$ was introduced into 150 mL of water, and then after the addition of 15 mL of NH_3 (25 wt %) with agitation under N_2 protection the Fe_3O_4 solid products were obtained at 50 °C for 30 min of reaction time.

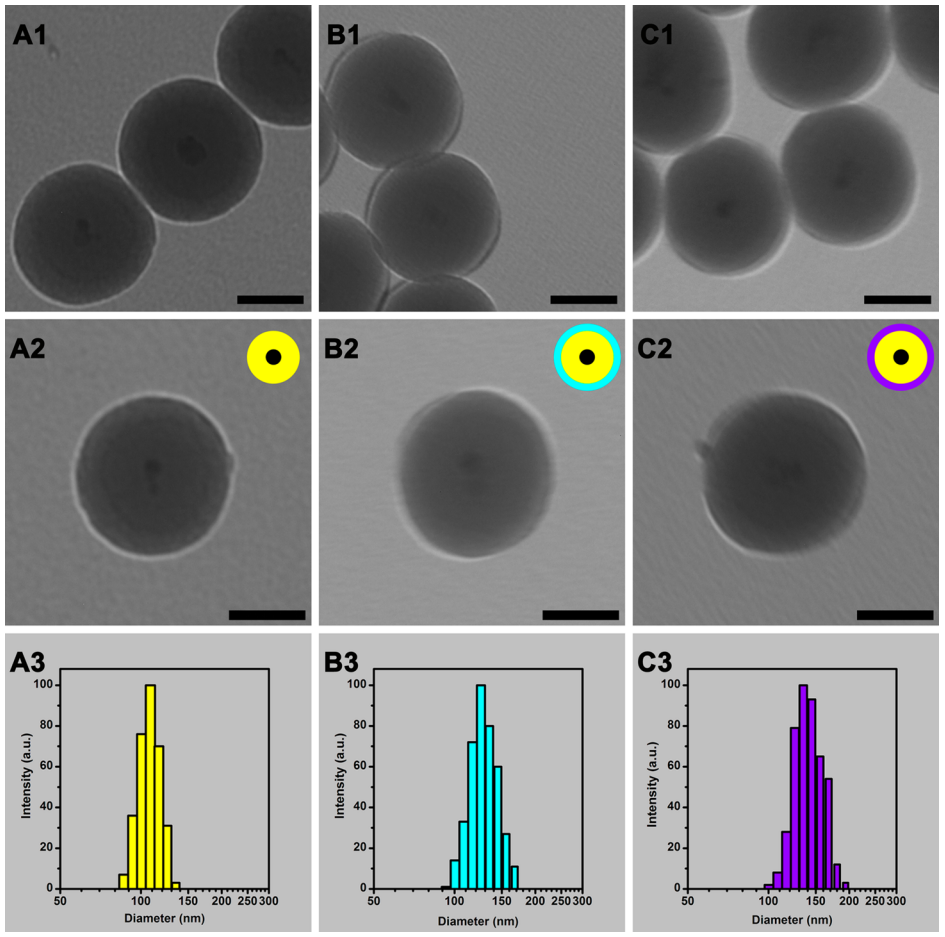

Figure 2. TEM images (1 and 2) and particle size distribution (3) of MS NPs (A), poly(ABBA-*co*-MMA) coated MS NPs (B), and BAMNH NPs (C).

Preparation of MS NPs. The MS NPs were prepared according to the stöber process.[27] An amount of 0.2 g of the Fe_3O_4 powder, 20 mL of water, 80 mL of ethanol, and 2 mL of NH_3 (25 wt %) were well mixed, and then 20 mL of TEOS (5 mL) in ethanol was added dropwise into the above-mentioned mixture. Finally, MS NPs were available with stirring at 25 °C for 12 h.

Preparation of Poly(5-allylbarbituric acid-*co*-methyl methacrylate) Coated MS NPs. Amounts of 0.5 g of MS NPs and 0.01 g of KPS were successively dispersed in 200 mL of water under the condition of ultrasonication. The 5-allylbarbituric acid/methyl methacrylate (ABBA/MMA, 0.05 g/0.95 g) mixture was then added, and MS NPs were encapsulated by poly(ABBA-*co*-MMA) at 75 °C for 24 h.

Preparation of BAMNH NPs. The as-prepared poly(ABBA-*co*-MMA) encapsulated MS NPs were well dispersed into the HClO solution (10%), and the chlorination reaction was performed in the neutral pH environment at 25 °C for 6 h. The obtained BAMNH NPs were purified with several times of washing to eliminate unreacted impurities.

Characterizations. TEM images were available from a Hitachi H-8100 transmission electron microscope at 200 kV. X-ray photoelectron spectra (XPS) measurement was taken on a PHI-5000CESCA system with Mg K radiation (hr = 1253.6 eV). The XRD patterns were collected on a Siemens model D5000 diffractometer equipped with a copper anode producing X-rays with a wavelength of 1.5418 Å. FTIR spectra were captured by using a Thermo Nicolet (Woburn, MA) Avatar 370 FTIR spectrometer. TGA was obtained by using a Perkin-Elmer thermogravimetric analyzer. Magnetization curves as a function of magnetic field were recorded at 298 K under magnetic field up to 10 kOe.

Antibacterial Test. Antibacterial experiment selected *S. aureus* (ATCC 25923, Gram-positive), *B. subtilis* (ATCC 6633, Gram-positive), *E. coli* (ATCC 25922, Gram-negative), and *P. aeruginosa* (ATCC 27853, Gram-negative) as model microorganisms. In the procedure, 50 μL of bacteria suspension with 10^{6-7} CFU/mL concentration was mixed with 450 μL of sample suspension, and then excessive $Na_2S_2O_3$ solution (0.03 wt %) was introduced to terminate the sterilization process after a certain contacting period. The as-prepared mixture was dispersed onto LB agar plates after serial dilution to incubate at 37 °C for 24 h. Samples with different serial concentrations were utilized to determine the minimum inhibitory concentration (MIC) by the same method mentioned above.

RESULTS AND DISCUSSION

The synthesis of the BAMNH NPs involves four steps as shown in Figure 1, and each step is well controlled. Barbituric acid derivative ABBA was synthesized from diethyl malonate by the cyclization reaction between urea and diethyl allylmalonate (Figure S1, Supporting Information) and characterized by ^{1}NMR (Figure S2A, Supporting Information). IO NPs prepared by the Massart method are first trapped within silica spheres using the well-known stöber process based on the hydrolysis of TEOS. The obtained MS NPs with Si−OH groups on the surfaces are hydrophilic, whereas ABBA/MMA mixtures are hydrophobic.[28] Thereby, monomers introduced into aqueous suspension are adsorbed dispersedly on the MS NP surface with vigorous stirring neither using surfactant nor stabilizer. Upon sequentially adding the initiator KPS into the

dx.doi.org/10.1021/am402191j | ACS Appl. Mater. Interfaces 2013, 5, 8125−8133

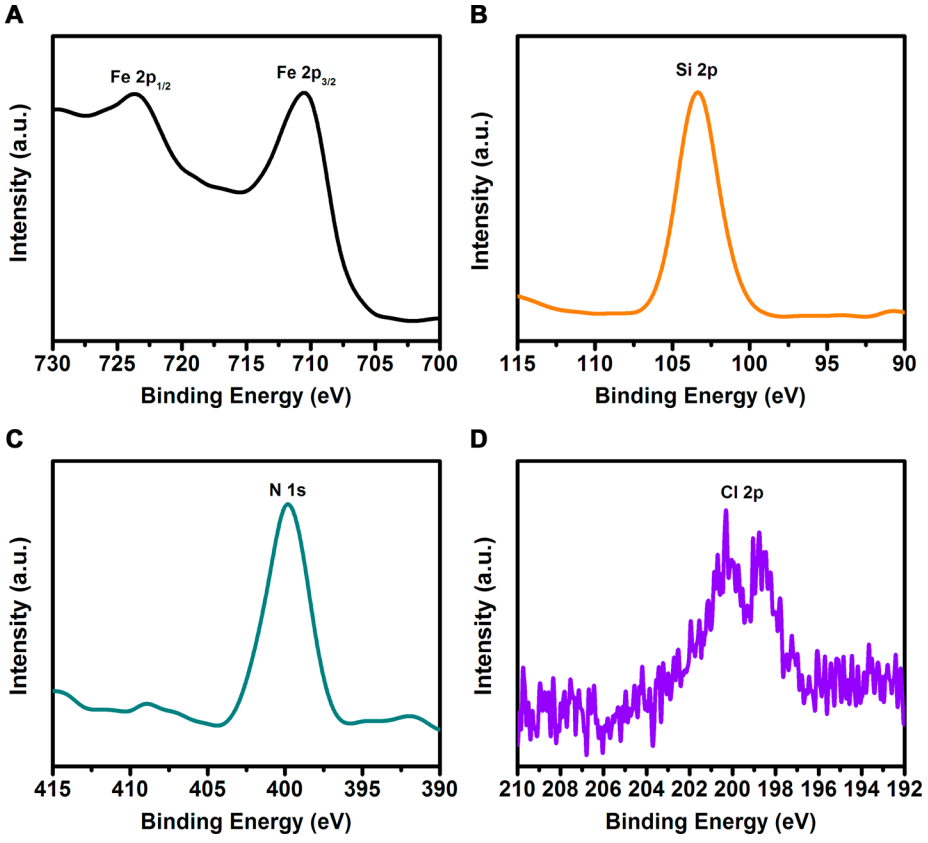

Figure 3. High-resolution XPS spectra of Fe 2p for IO NPs (A), Si 2p for MS NPs (B), N 1s for poly(ABBA-*co*-MMA)-coated MS NPs (C), and Cl 2p for BAMNH NPs (D).

complex solution, polymeric shells are quickly formed from the outer surface toward the center, while the MS NPs stay inside as core components, producing core−shell nanoparticles. It is difficult to prepare a high molecular weight ABBA homopolymer through radical polymerization due to its autoinhibition mechanism from an allylic structure.[29] Therefore, we selected MMA as the comonomer with ABBA because the ester group of MMA is favorable to radical polymerization, which can enhance the chain propagation reaction of ABBA during the radical polymerization.[30] Copolymerization of ABBA with MMA without MS NPs support was carried out as well for a better understanding of the compositions of copolymers, and the product polymer was characterized by ^{1}H NMR and FTIR. Figure S2 and Figure S3 (Supporting Information) well confirm the formation of poly(ABBA-*co*-MMA) via the radical copolymerization of ABBA with MMA, suggesting a higher activity of ABBA towards the chain propagation direction with the introduction of comonomer MMA. The barbituric acid moieties of the polymer shell are transformed into *N*-halamine structure by immersion in sodium hypochlorite solution. Halogenated derivatives of barbituric acid belong to the class of cyclic *N*-halamines, which return back to the initial barbituric acid moieties after antibacterial performance, and *N*-halamines are recovered after another bleach treatment. Introducing MS NPs as templates for preparation of BAMNH NPs not only achieves the target of enlarging the activated surface area but also realizes the recycling of the antibacterial agents.

Precise control of BAMNH NPs in well-defined core−shell structure with desirable size and shell thickness can be readily achieved. The morphology and particle size distribution of the products are studied by TEM. As indicated in Figure S4 and Figure S5 (Supporting Information), IO NPs have spherical shape with sizes in the range of 7−30 nm. One can see that MS NPs in Figure 2A1 and A2 have typical spherical shape with average diameter of 108.5 nm, and the magnetic IO NPs orderly exist in the center of the particles. The silica coating can effectively prevent the IO NPs from magnetically induced aggregation and surface oxidation and thus well increase their stability. The silica shell can also provide abundant Si−OH groups on smooth surfaces, which favor the sequential polymer encapsulation thanks to their hydrophilic property. In Figure 2B1 and B2, typical spherical shape, core−shell structure, and smooth surface are noticed in polymer-coated MS NPs, and the shell thickness of the outer polymer coated on the raw materials is about 8.5 nm. After chlorination, the BAMNH NPs with average diameter of 134.9 nm display a somewhat rough surface in Figure 2C1 and C2 probably because of the N−H → N−Cl transformation in barbituric acid moieties, whereas the sample keeps original morphology and structure, which verifies that bleach treatment has no remarkable influence on the inner magnetic silica component. Figure 2A3, B3, and C3 further shows that the sizes of all these three samples are uniform and that the size distribution is narrow.

XPS measurement was carried out to access the surface composition, and Fe 2p from IO NPs, Si 2p from MS NPs, N 1s from poly(ABBA-*co*-MMA)-coated MS NPs, and Cl 2p from BAMNH NPs spectra were provided in Figure 3.[31−34] The presence of these peaks identifies the successful formation of the characteristic bonds in each synthetic step. The chemical bonds of BAMNH NPs are further illustrated in Figure 4 from the magnified C 1s and O 1s peaks. The C 1s peak was curved into four peak components, which were attributed to the C−C,

dx.doi.org/10.1021/am402191j | ACS Appl. Mater. Interfaces 2013, 5, 8125−8133

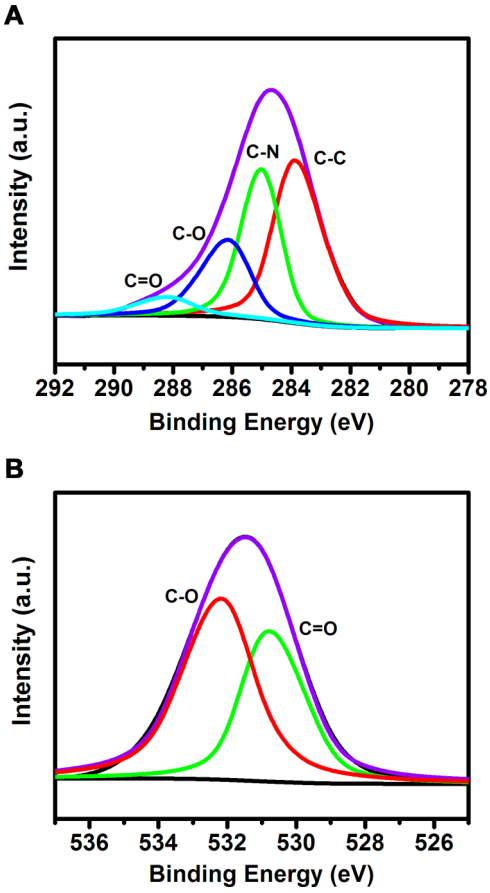

Figure 4. High-resolution XPS spectra of C 1s (A) and O 1s (B) for BAMNH NPs.

C−N, C−O, and C═O groups, respectively.[35] The curve fitting of O 1s revealed two separate peaks corresponding to the C−O and C═O bond, respectively.[36] The C 1s and O 1s spectrum not only exhibits the surface chemistry but also further verifies the successful formation of BAMNH NPs.

The XRD pattern of the BAMNH NPs reveals diffraction peaks corresponding to the magnetic cubic structure of standard Fe_3O_4 reflections shown in Figure S6 (Supporting Information).[37] From 15° to 25° in the XRD pattern, there exists a strong and broad peak attributed to the amorphous silica and *N*-halamine.[38] However, XRD analysis does not provide detailed information about silica and polymeric *N*-halamine components. Therefore, the existence of silica and *N*-halamine coating was characterized by FTIR (Figure 5B). In the FTIR spectrum, besides the Fe−O bond from Fe_3O_4 that appeared around 530 cm^{-1},[39] peaks at around 800, 950, 1100, 1450, 2980, 2930, 1390, and 760 were attributed to the Si−O−Si, Si−OH, and $SiOCH_3$ from the silica shell and C−H and N−Cl bonds from the outer *N*-halamine shell.[40,41] The stretching vibration peak of the hydroxyl group and residual water appeared at 3570 and 1635 cm^{-1}, respectively.[42,43] The weak N−H peak at around 3240 cm^{-1} is possibly corresponding to the unchlorinated barbituric acid moieties in the inner layer.[41] These data completely confirmed the formation of BAMNH NPs. TGA was carried out for quantitative analysis of the *N*-halamine content in the BAMNH NPs shown in Figure 5C. From the TGA result, it was concluded that the resultant nanoparticles consisted of 11 wt % polymeric *N*-halamine.

Magnetic property provides a rapid and convenient means for the separation of *N*-halamine composites, being free of the repeated centrifugation for practical applications. Figure 5D presents the hysteresis loop of BAMNH NPs, which displayed superparamagnetic performance. BAMNH NPs have a saturation magnetization value of 1.8 $emu \cdot g^{-1}$, which is less than that of the pristine magnetic IO NPs (Figure S7, Supporting Information).[44] The diamagnetic contribution from the silica shell and the decreased magnetic moment for *N*-halamine surrounding MS NPs are the explanation for the reduced saturation magnetization value.[45] However, this is sufficient for magnetic separation of antibacterial *N*-halamine from water solution by a magnetic field within a few seconds (inset in Figure 5D), which is beneficial to the recyclable application in the antimicrobial field.

It can be expected that BAMNH NPs have potent antibacterial capabilities originating from the antibacterial *N*-halamine shell, and the magnetic core provides recyclable biocidal performances. The antimicrobial activity of BAMNH NPs with chlorine content of 2.54% was assessed by the diameter of inhibition zone (DIZ) test with *E. coli* as the representative microorganism. DIZ results reflect the susceptibility of the bacteria towards BAMNH NPs. For comparison, the bulk powder *N*-halamine with chlorine content of 2.87% was fabricated by the same polymerization method without MS NPs, and the DIZ values of the control, MS NPs, and bulk powder *N*-halamine were illustrated as well. Figure 6 displays the optical images of the DIZ result against *E. coli* for each sample. Robust growth of *E. coli* was vividly observed in control experiments. Same as the control, MS NPs had no considerable antibacterial activity, indicating that the support component was not toxic to the bacteria. Unlike the former, the bulk powder *N*-halamine and BAMNH NPs showed a palpable DIZ value indicating significant antibacterial activity against *E. coli*. We can hence predicate that excellent biocidal function of BAMNH NPs is derived from the *N*-halamine structure. The average DIZ value for BAMNH NPs was 26 mm, while the corresponding value for the bulk counterpart was merely 20 mm, suggesting that BAMNH NPs have more effective contact biocidal property than the bulk powder *N*-halamine. The large surface area of BAMNH NPs compared with their bulk counterparts is the best explanation for the improved antimicrobial performance.

The antibacterial properties of the as-prepared BAMNH NPs with chlorine content of 2.54% were assessed quantitatively by a biocidal kinetic test shown in Figure 7. *S. aureus* (typical Gram-positive bacteria) and *P. aeruginosa* (typical Gram-negative bacteria) were selected for antibacterial experiments. The number of surviving bacterial colonies of both bacteria was reduced as the contact time increased. BAMNH NPs inactivated 73% *P. aeruginosa* and 55% *S. aureus* only within 5 min. The inset photographs in Figure 7 displayed that the small white dots on the culture plates representing the bacterial colonies drastically reduced after 60 min exposure to the BAMNH NPs. Pristine MS NPs and bulk powder *N*-halamine with chlorine content of 2.87% were also introduced for the antibacterial test (Figure S8, Supporting Information). The control and MS NPs showed the same result after 60 min contact with bacteria, whereas bulk powder *N*-halamine displayed obvious antibacterial activity, suggesting that MS NP templates have no biocidal function at all, and *N*-halamine structures offer BAMNH NP antimicrobial property. However, BAMNH NPs with nanosize displayed much more antibacterial

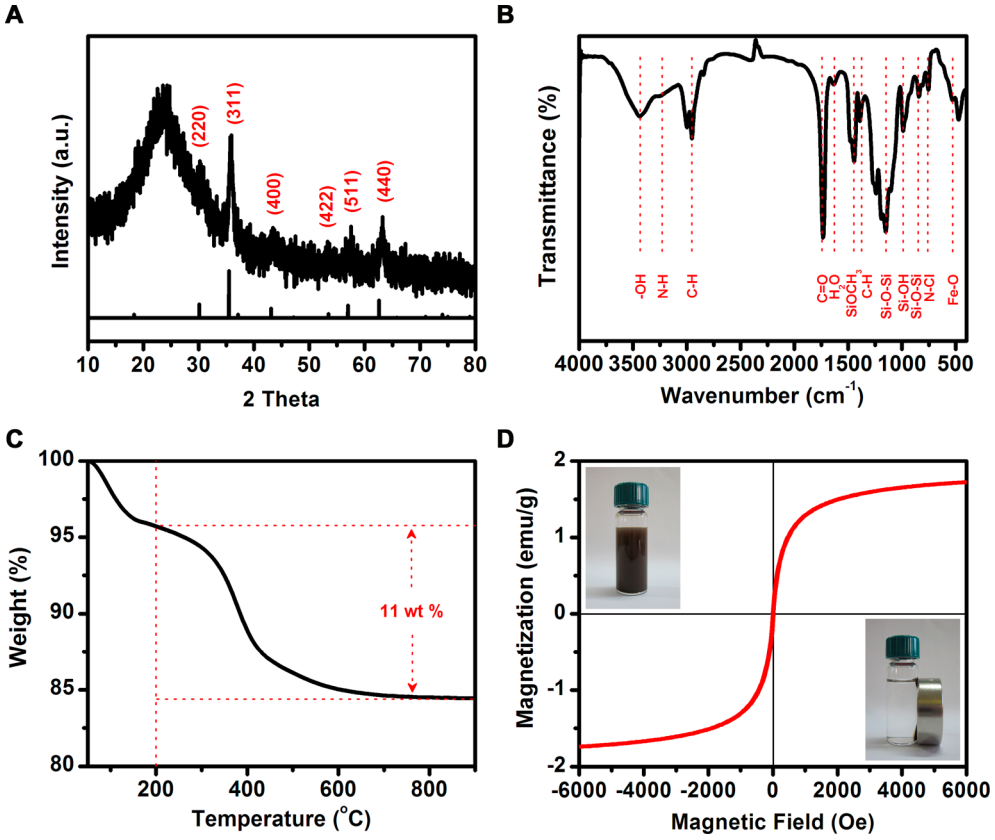

Figure 5. XRD (A), FTIR (B), TGA (C), and magnetization property (D) of BAMNH NPs. Inset in (D) is a photograph of BAMNH NPs dispersed in aqueous solution without and with an external magnetic field.

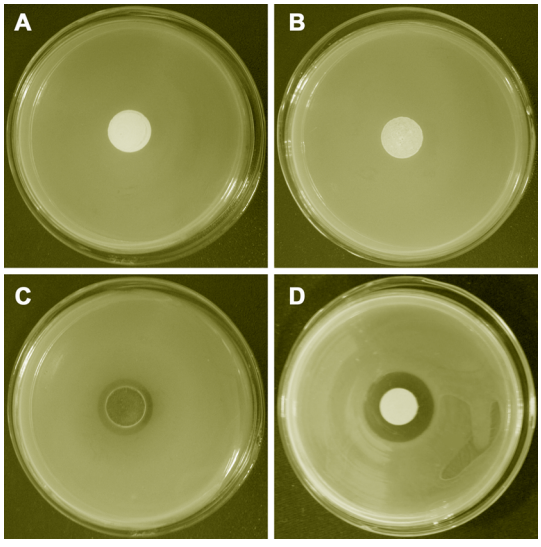

Figure 6. Optical images of the zone of inhibition against *E. coli* for the control (A), MS NPs (B), bulk powder *N*-halamine (C), and BAMNH NPs (D).

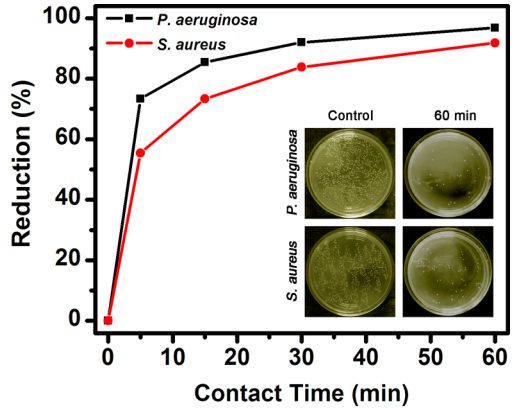

Figure 7. Antibacterial kinetic test graphs for BAMNH NPs against *P. aeruginosa* and *S. aureus*. Inset is photographs showing the bacterial culture plates of *P. aeruginosa* and *S. aureus* upon a 60 min exposure of the control and BAMNH NPs.

capability than bulk counterparts because antibacterial materials with smaller size can provide larger surface area to contact with the bacteria.

In our previous report, several kinds of *N*-halamine nanoparticles based on the hydantoin derivative were successfully fabricated, and their biocidal activities were systematically assessed.[46−48] To substantiate the structural effect, the antimicrobial activity of BAMNH NPs originated from the barbituric acid derivative was quantitatively compared with hydantoin-structural magnetic *N*-halamine nanoparticles (HMNH NPs) with chlorine content of 2.63% in this report. The MIC means the sample concentration corresponding to the reduction of ≥3 log in the CFU/mL colony numbers. As shown in Table 1, MIC values against different model bacteria were determined by the agar plate method. MIC values of BAMNH NPs corresponding to *S. aureus*, *B. subtilis*, *E. coli*, and *P. aeruginosa* are 80, 80, 80, and 40, respectively, and the MIC values of 160, 160, 160, and 80 are observed for HMNH NPs. It is obvious that BAMNH NPs displayed much higher antibacterial efficiency versus HMNH NPs. This phenomenon

Table 1. Minimum Inhibitory Concentration (MIC) of HMNH NPs and BAMNH NPs Against *S. aureus*, *B. subtilis*, *E. coli*, and *P. aeruginosa*

	MIC (mg/mL)			
	Gram-positive bacteria		Gram-negative bacteria	
sample	*S. aureus*	*B. subtilis*	*E. coli*	*P. aeruginosa*
HMNH NPs	160	160	160	80
BAMNH NPs	80	80	80	40

may be assigned to the structure difference between barbituric acid-based and hydantoin-originated *N*-halamine. It is reported that *N*-halamine shows the antibacterial power in an order of imide > amide > amine halamine.[8] Barbituric acid derivatives are heterocyclic compounds with two imide groups in the structure, while hydantoin compounds have one imide and one amide group. For this reason, it is considered that barbituric acid-based *N*-halamine would be more powerful than hydantoin-based *N*-halamine.

The washing stability and storage stability of BAMNH NPs and HMNH NPs were comparatively studied as well. As shown in Table 2, the stability of the *N*-halamine coating on MS NPs

Table 2. Stability of BAMNH NPs and HMNH NPs toward Repeated Laundering

	chlorine content (wt %)	
laundering cycles	BAMNH NPs	HMNH NPs
0	2.54	2.63
2	2.47	2.58
4	2.42	2.51
6	2.38	2.47
8	2.33	2.43
10	2.31	2.39

toward repeated laundering was estimated by determining the remaining chlorine content of the sample. In general, *N*-halamine coating on MS NPs displayed promising washing stability. Chlorine content was reduced merely from 2.54% to 2.31% for BAMNH NPs and from 2.63% to 2.39% for HMNH NPs. More than 90% remaining chlorine content was obtained for both BAMNH NPs and HMNH NPs even after 10 washing cycles. The storage stability of BAMNH NPs and HMNH NPs in sealed conditions of 25 °C and 65 % RH was also assessed through the quantification of the remaining chlorine content over a 15 day period. Both these samples retained around 95% of the initial chlorine loading after 15 days storage, and almost the whole initial chlorine was restored upon rechlorination treatment, suggesting that N−Cl bond dissociation causes the loss of chlorine loading rather than leaching out of the polymer coating.

Antimicrobial action of *N*-halamine involves a halogen transfer process from *N*-halamines to bacterial cells. Therefore, chlorine content is a decisive factor of *N*-halamine governing the antibacterial activity. The BAMNH NPs with different chlorine content (0.35%, 0.47%, 0.66%, 1.08%, 1.75%, and 2.54%) were fabricated to explore the effect on antibacterial efficiency. Table S1 (Supporting Information) summarizes the synthetic conditions of BAMNH NPs with different chlorine loading. The relationship between the chlorine content and biocidal activity is illustrated by means of the bacterial colonies reduction as shown in Figure 8. Overall, the sample with higher chlorine loading reveals stronger antibacterial activity. A 0.35%

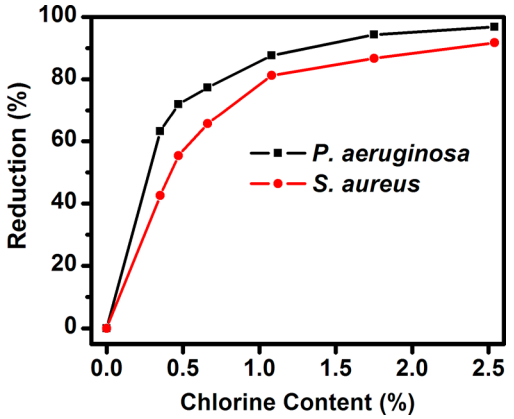

Figure 8. Reduction of bacterial colonies (*S. aureus* and *P. aeruginosa*) after the exposure to the BAMNH NPs with different chlorine content.

chlorine loaded sample can merely provide 43% *S. aureus* reduction, while a sample containing 2.54% chlorine can kill 92% *S. aureus* bacterial colonies within 60 min. The reduction of *P. aeruginosa* increased from 63% to 97% with increasing chlorine content from 0.35% to 2.54%, showing the similar biocidal trend with *S. aureus*. It is assumed that the antimicrobial activity of *N*-halamine is proportional to chlorine loading because a high chlorine content sample can offer more biocidal contact sites with bacteria and thus provide enhanced antibacterial efficiency. The antibacterial assessment of BAMNH NPs with different chlorine content mentioned above proves this hypothesis. Interestingly, the number of bacterial colonies reduced drastically at first, and then a leveling effect appeared as the chlorine content was further increased. The possible reason was illustrated as follows. The target *N*-halamine materials were obtained through the N−H → N−Cl transformation of the polymeric shell, which is performed from the outer surface to the inner shell with the condition of the bleach solution during the chlorination treatment. The imide groups of barbituric acid derivative in the inner shell can hardly transform completely into an *N*-halamine structure with lower chlorine content, leading to the incomplete chlorine process. When the chlorine content was increased adequately, the N−H → N−Cl transformation occurred completely, and chlorine content was kept constant even with excess chlorination treatment. In the case of *N*-halamine, antimicrobial performance strongly depends on the contact between the biocide and the bacteria, and thus the inner N−Cl groups can hardly provide antibacterial function directly. For another, higher hydrophobicity of BAMNH NPs is also an explanation for the leveling effect with higher chlorine loading, which can cause poorer contact of the sample with the bacteria. Thereby, the antibacterial efficiency dramatically increases first and calm downs with increasing chlorine content.

As discussed above, potential recyclability is one of the main advantages of BAMNH NPs compared with other antibacterial materials. In this case, the magnetic property of MS NPs support could be exploited to remove the target after antibacterial behavior and make the reclaimed substance ready for a new antibacterial cycle. Recycle application of BAMNH NPs was schematically illustrated in Figure 9A. *N*-Halamines, as regenerable antibacterial agents, returned to their barbituric acid precursors as they contact with the microorganism, and *N*-halamines are recovered after the simple bleach treatment. Thanks to the super-paramagnetic substrate,

dx.doi.org/10.1021/am402191j | ACS Appl. Mater. Interfaces 2013, 5, 8125−8133

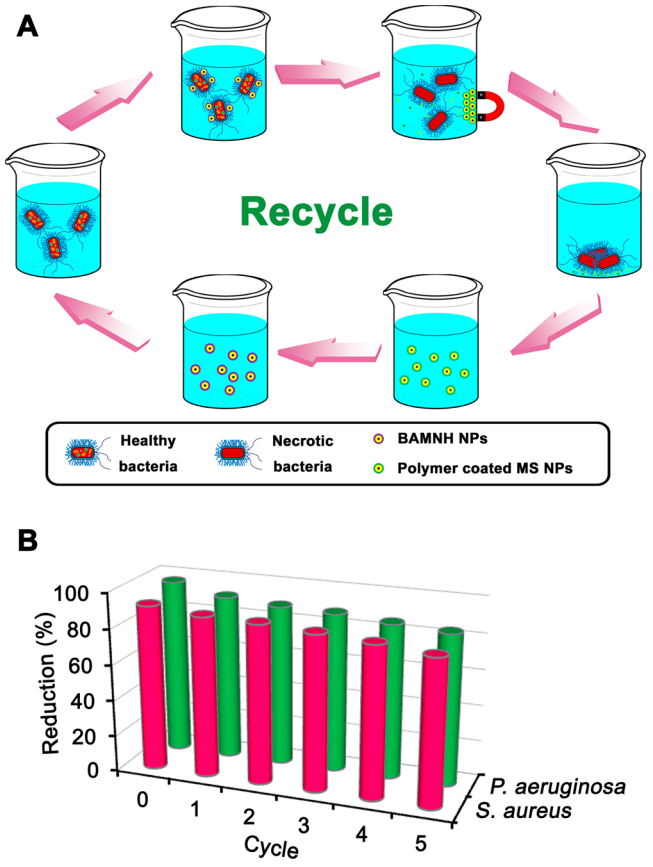

Figure 9. (A) Schematic depiction of the recycle antibacterial application of the BAMNH NPs. (B) Antibacterial activity of BAMNH NPs against *P. aeruginosa* and *S. aureus* during five antibacterial cycles.

the BAMNH NPs can be easily recovered in the external magnetic field. TEM and IR techniques were introduced to confirm the stability of BAMNH NPs in morphology and structure during the recycle application as shown in Figure S9 (Supporting Information). No significant change was observed between the TEM image of BAMNH NPs (Figure 2C1 and C2) and the corresponding image after several recycle procedures (Figure S9A, Supporting Information). As for IR spectra, BAMNH NPs still have their original characteristic peaks after recycle application (Figure S9B, Supporting Information). Furthermore, the recovered *N*-halamine nanoparticles were examined to confirm the repeatability of their antibacterial functions. The antibacterial activity remains stable even after five cycles of antimicrobial tests for magnetic *N*-halamine nanoparticles. As shown in the recycle graph in Figure 9B, BAMNH NPs still had a distinguishable antibacterial efficiency, and no significant decrease was observed in antibacterial capability after five recycle experiments.

CONCLUSION

In summary, barbituric acid-based magnetic *N*-halamine nanoparticles (BAMNH NPs) with average diameters of ca. 120 nm were obtained with MS NPs as the core and barbituric acid-based *N*-halamine as the shell. Magnetic silica nanoparticles served as a template for the well-defined spherical particles with uniform-sized Fe_3O_4 orderly existing in the center of the silica spheres. After *N*-halamine modification, the resultant nanoparticles showed distinct core–shell structure with 11 wt % polymeric *N*-halamine and shell thickness of 10 nm. BAMNH NPs with the saturation magnetization value of 1.8 emu·g^{-1} displayed superparamagnetic performance. Antimicrobial tests showed that BAMNH NPs exhibit higher biocidal activity than the bulk powder *N*-halamine. Owing to the structural difference, BAMNH NPs have a significant advantage over hydantoin-based *N*-halamine nanoparticles. Besides, BAMNH NPs also exhibited promising stability toward repeated laundering and long-term storage. Furthermore, BAMNH NPs with different chlorine content were comparatively chosen to verify the hypothesis that the bactericidal capability is proportional to chlorine loading. A recycle antibacterial test revealed that BAMNH NPs can maintain the distinguishable antibacterial performance after five recycle experiments.

ASSOCIATED CONTENT

Supporting Information

Synthetic route of 5-allylbarbituric acid; ^{1}H NMR and FTIR of 5-allylbarbituric acid, methyl methacrylate, and poly(5-allylbarbituric acid-*co*-methyl methacrylate); TEM photograph, distribution of particle size, XRD pattern, and the magnetic hysteresis loop of pristine IO NPs; Antibacterial function of the control, pristine MS NPs, and bulk powder *N*-halamine; TEM photograph and IR spectra of BAMNH NPs after several antibacterial recycle; Synthetic condition of BAMNH NPs with different chlorine content. This material is available free of charge via the Internet at http://pubs.acs.org.

AUTHOR INFORMATION

Corresponding Author

*E-mail: dongali@imu.edu.cn. Tel.: +86 471 4992982.

Notes

The authors declare no competing financial interest.

ACKNOWLEDGMENTS

This research was supported by the National Natural Science Foundation of China (31160332 and 21263009), the National Natural Science Foundation of Jilin Province (201115011), and the Supported by Program of Higher-level Talents of Inner Mongolia University (30105-125136).

REFERENCES

(1) Blanazs, A.; Verber, R.; Mykhaylyk, O. O.; Ryan, A. J.; Heath, J. Z.; Douglas, C. W. I.; Armes, S. P. *J. Am. Chem. Soc.* **2012**, *134*, 9741–9748.
(2) Hu, B.; Zhang, L.; Chen, X.; Wang, J. *Nanoscale* **2013**, *5*, 246–252.
(3) Wang, L.; Erasquin, U. J.; Zhao, M.; Ren, L.; Zhang, M. Y.; Cheng, G. J.; Wang, Y.; Cai, C. *ACS Appl. Mater. Interfaces* **2011**, *3*, 2885–2894.
(4) Kocer, H. B.; Cerkez, I.; Worley, S. D.; Broughton, R. M.; Huang, T. S. *ACS Appl. Mater. Interfaces* **2011**, *3*, 3189–3194.
(5) Kocer, H. B.; Worley, S. D.; Broughton, R. M.; Huang, T. S. *React. Funct. Polym.* **2011**, *71*, 561–568.
(6) Padmanabhuni, R. V.; Luo, J.; Cao, Z.; Sun, Y. *Ind. Eng. Chem. Res.* **2012**, *51*, 5148–5156.
(7) Dong, A.; Lan, S.; Huang, J.; Wang, T.; Zhao, T.; Wang, W.; Xiao, L.; Zheng, X.; Liu, F.; Gao, G.; Chen, Y. *J. Colloid Interface Sci.* **2011**, *346*, 333–340.
(8) Barnes, K.; Liang, J.; Wu, R.; Worley, S. D.; Lee, J.; Broughton, R. M.; Huang, T. S. *Biomaterials* **2006**, *27*, 4825–4830.

(9) Dorofeeva, E. O.; Elinson, M. N.; Vereshchagin, A. N.; Stepanov, N. O.; Bushmarinov, I. S.; Belyakov, P. A.; Sokolova, O. O.; Nikishin, G. I. *RSC Adv.* **2012**, *2*, 4444−4452.
(10) Ahmed, A. E. I.; Hay, J. N.; Bushell, M. E.; Wardell, J. N.; Cavalli, G. *React. Funct. Polym.* **2008**, *68*, 248−260.
(11) Ahmed, A. E. I.; Hay, J. N.; Bushell, M. E.; Wardell, J. N.; Cavalli, G. *React. Funct. Polym.* **2008**, *68*, 1448−1458.
(12) Griffiths, J.; Maliha, B.; Moloney, M. G.; Thompson, A. L. *Langmuir* **2010**, *26*, 14142−14153.
(13) Kocer, H. B. *Prog. Org. Coat.* **2012**, *74*, 100−105.
(14) Hui, C.; Shen, C.; Tian, J.; Bao, L.; Ding, H.; Li, C.; Tian, Y.; Shi, X.; Gao, H. *Nanoscale* **2011**, *3*, 701−705.
(15) Pang, H.; Lu, Q.; Li, Y.; Gao, F. *Chem. Commun.* **2009**, 7542−7544.
(16) Li, Y.; Ding, M.; Wang, S.; Wang, R.; Wu, X.; Wen, T.; Yuan, L.; Dai, P.; Lin, Y.; Zhou, X. *ACS Appl. Mater. Interfaces* **2011**, *3*, 3308−3315.
(17) Li, D.; Tech, W. Y.; Woodward, R. C.; Cashion, J. D.; Selomulya, C.; Amal, R. *J. Phys. Chem. C* **2009**, *113*, 12040−12047.
(18) Shavel, A.; Rodríguez-González, B.; Spasova, M.; Farle, M.; Liz-Marzán, L. M. *Adv. Funct. Mater.* **2007**, *17*, 3870−3876.
(19) Zhao, L.; Chi, Y.; Yuan, Q.; Li, N.; Yan, W.; Li, X. *J. Colloid Interface Sci.* **2013**, *390*, 70−77.
(20) Ding, H. L.; Zhang, Y. X.; Wang, S.; Xu, J. M.; Xu, S. C.; Li, G. H. *Chem. Mater.* **2012**, *24*, 4572−4580.
(21) Teng, Z.; Su, X.; Chen, G.; Tian, C.; Li, H.; Ai, L.; Lu, G. *Colloids Surf. A* **2012**, *402*, 60−65.
(22) He, L.; Malik, V.; Wang, M.; Hu, Y.; Anson, F. E.; Yin, Y. *Nanoscale* **2012**, *4*, 4438−4442.
(23) Zhou, L.; Gao, C.; Xu, W. *ACS Appl. Mater. Interfaces* **2010**, *2*, 1483−1491.
(24) Lanners, S.; Norouzi-Arasi, H.; Khiri, N.; Hanquet, G. *Eur. J. Org. Chem.* **2007**, 4065−4075.
(25) Ishikawa, I.; Khachatrian, V. E.; Melik-Ohanjanian, R. G.; Kawahara, N.; Mizuno, Y.; Ogura, H. *Chem. Pharm. Bull.* **1992**, *40*, 846−850.
(26) Occhiponti, E.; Verderio, P.; Natalello, A.; Galbiati, E.; Colombo, M.; Mazzucchelli, S.; Salvadè, A.; Tortora, P.; Doglia, S. M.; Prosperi, D. *Nanoscale* **2011**, *3*, 387−390.
(27) Du, P.; Wang, T.; Liu, P. *Colloids Surf. B* **2013**, *102*, 1−8.
(28) Tiraferri, A.; Kang, Y.; Giannelis, E. P.; Elimelech, M. *ACS Appl. Mater, Interfaces* **2012**, *4*, 5044−5053.
(29) Sun, Y.; Sun, G. *J. Appl. Polym. Sci.* **2001**, *80*, 2460−2467.
(30) Jang, J.; Kim, Y. *Chem. Commun.* **2008**, 4016−4018.
(31) Tian, Y.; Yu, B.; Li, X.; Li, K. *J. Mater. Chem.* **2011**, *21*, 2476−2481.
(32) Deng, Z.; Chen, M.; Wu, L. *J. Phys. Chem. C* **2007**, *111*, 11692−11698.
(33) Xuan, S.; Wang, Y. J.; Leung, K. C.; Shu, K. *J. Phys. Chem. C* **2008**, *112*, 18804−18809.
(34) Wang, X.; Wang, C.; Zhang, D. *Mater. Lett.* **2012**, *72*, 12−14.
(35) Khai, T. V.; Na, H. G.; Kwak, D. S.; Kwon, Y. J.; Ham, H.; Shim, K. B.; Kim, H. W. *J. Mater. Chem.* **2012**, *22*, 17992−18003.
(36) Ma, J.; Wang, J. N.; Wang, X. X. *J. Mater. Chem.* **2009**, *19*, 3033−3041.
(37) Ogawa, T.; Takahashi, Y.; Yang, H.; Kimura, K.; Sakurai, M.; Takahashi, M. *Nanotechnology* **2006**, *17*, 5539−5543.
(38) Liu, J.; Zhang, L.; Shi, S.; Chen, S.; Zhou, N.; Zhang, Z.; Cheng, Z.; Zhu, X. *Langmuir* **2010**, *26*, 14806−14813.
(39) Huang, Z.; Tang, F. *J. Colloid Interface Sci.* **2005**, *281*, 432−436.
(40) Xu, Z.; Li, C.; Kang, X.; Yang, D.; Yang, P.; Hou, Z.; Lin, J. *J. Phys. Chem. C* **2010**, *114*, 16343−16350.
(41) Chen, Z.; Sun, Y. *Ind. Eng. Chem. Res.* **2006**, *45*, 2634−2640.
(42) Xu, P.; Wang, H.; Tong, R.; Du, Q.; Zhong, W. *Colloid Polym. Sci.* **2006**, *284*, 755−762.
(43) Freris, I.; Gristofori, D.; Riello, P.; Benedetti, A. *J. Colloid Interface Sci.* **2009**, *331*, 351−355.
(44) Chen, F. H.; Gao, Q.; Ni, J. Z. *Nanotechnology* **2008**, *19*, 165103.
(45) Guo, J.; Yang, W.; Wang, C.; He, H.; Chen, J. *Chem. Mater.* **2006**, *18*, 5554−5562.
(46) Dong, A.; Zhang, Q.; Wang, T.; Wang, W.; Liu, F.; Gao, G. *J. Phys. Chem. C* **2010**, *114*, 17298−17303.
(47) Dong, A.; Huang, J.; Lan, S.; Wang, T.; Xiao, L.; Wang, W.; Zhao, T.; Zheng, X.; Liu, F.; Gao, G.; Chen, Y. *Nanotechnology* **2011**, *22*, 295602.
(48) Dong, A.; Lan, S.; Huang, J.; Wang, T.; Zhao, T.; Xiao, L.; Wang, W.; Zheng, X.; Liu, F.; Gao, G.; Chen, Y. *ACS Appl. Mater. Interfaces* **2011**, *3*, 4228−4235.